QUASI-STATIC ROCK MECHANICS DATA FOR ROCKSALT FROM

THREE STRATEGIC PETROLEUMRESERVE DOMES*

Ronald H. Price, Wolfgang R. Wawersik, David W. Hannum & Jeffrey A. Zirzow
Sandia National Laboratories**
Albuquerque, New Mexico 87185

ABSTRACT

Triaxial compression and extension experiments have been run on rock-salt samples from three Strategic Petroleum Reserve (SPR) domes. Seventeen quasi-static tests were loaded at mean stress rates of .66-1.04 psi/sec (4.5-7.2 kPa/sec), confining pressures of 14.5-2000 psi (0.1-13.8 MPa) and temperatures of 22-100°C. Eleven of the test specimens were from Bryan Mound, Texas, and three each were from Bayou Choctaw, Louisiana, and West Hackberry, Louisiana.

In general, the resulting mechanical data from the three domes are similar, and they are consistent with previously published data. Ultimate sample strengths are directly related to confining pressure (least principal stress) and indirectly related to temperature, while ductility increases with both pressure and temperature.

TABLE OF CONTENTS

LIST OF SYMBOLS AND CONVENTIONS

$\sigma_1, \sigma_2, \sigma_3$	True principal stresses (force/current area); compressive stresses are positive
e_1, e_2, e_3	Natural or logarithmic principal strains (change in length/current length); compressive strains are positive
$e = e_1 + e_2 + e_3$	Volumetric strain
$\sigma_1 - \sigma_3$	Principal stress difference or differential stress
$e_1 - e_3$	Principal strain difference or differential strain
$(\sigma_1 - \sigma_3)_m$	Maximum differential stress
$(\sigma_1 - \sigma_3)_u$	Ultimate differential stress
$(e_1)_m, (-e_3)_m,$ $(e_1 - e_3)_m, (e)_m$	Natural strain values corresponding to $(\sigma_1 - \sigma_3)_m$
E, ν, G, K	Elastic moduli (Young's modulus, Poisson's ratio, shear modulus, bulk modulus)
T	Temperature

Experimental data are given in both English and metric units, but are plotted in English units consistent with SPR project requests.

<u>LIST OF TABLES</u>

Page

LIST OF FIGURES

<div align="right">

Page

</div>

LIST OF FIGURES (Cont'd.)

QUASI-STATIC ROCK MECHANICS DATA FOR **ROCKSALT** FROM

THREE STRATEGIC PETROLEUMRESERVE DOMES

Ronald H. Price, Wolfgang R. Wawersik, David W. Hannum & Jeffrey A. **Zirzow**
Sandia National Laboratories
Albuquerque, New Mexico 87185

INTRODUCTION

The U. S. Strategic Petroleum Reserve (SPR) program is actively storing crude oil within salt domes along the Texas-Louisiana coastline. Mechanical properties on **rocksalt** are needed to aid in the design and certification of the storage caverns. In the latest series of short-term deformation experiments, seventeen samples from three separate SPR domes were tested under quasi-static loading conditions. These tests on Bayou Choctaw, Bryan Mound and West Hackberry core were designed to evaluate the effects of changes in confining pressure, temperature and loading conditions on mechanical behavior as a part of a long-range effort to (1) establish the mechanical response of **rocksalt** from different SPR sites and (2) assess the fracture potential of **rocksalt** within the walls of the storage caverns.

SITE AND SAMPLE PREPARATION

General

Bayou Choctaw, Bryan Mound, and West Hackberry domes are all diapiric structures formed from Jurassic salt rising into the **Cenezoic** sedimentary units of the Texas-Louisiana coastline along the Gulf of Mexico. The samples used in mechanical testing are from raw core approximately 4 in (10.2 **cm)**in diameter taken during drilling at potential cavern sites.

Bayou Choctaw (BC)

· The Bayou Choctaw dome is located in **Iberville** Parish in south-central Louisiana. The large piercement structure is almost circular in horizontal cross-section. The three BC cores tested were from depths 2576-2581 **ft (785.1-786.7** m) in **drillhole 19A.** All of the samples contained medium mean grain sizes of **.31-.59** in (8-15 mm) with low standard deviations of **.16-.28** in (4-7 mm). Although no chemical and mineralogical sample data . were available, the samples appeared to be primarily **(> 90%)** halite (sodium chloride)with the predominant impurity probably being anhydrite. No preferential orientations of elongated grains or impurities were observed within any of these particular **rocksalt** specimens.

Bryan Mound (BM)

The Bryan Mound dome occurs within Brazoria County, Texas, one half mile from the coast of the Gulf of Mexico. This structure is also quite . . circular, with **a** relatively flat top at an approximate depth of **1100** ft (335 m). Experimental samples were obtained from the three **drillholes 107C** (1 sample), **110A** (6) and **110B (4),** at depth intervals of **2512 ft** (756.6 m), **2683.5-2692** ft **(817.9-820.5** m) and **3723-3728** ft **(1135-1136** m), respectively. Grain sizes varied between **.039** in (1 mm) and 1.7 in (43 **mm)** with an overall mean grain size of approximately **.33** in (8.5 **mm). Three** samples **(110A/2688.5, 110A/2692, 110B/3724)** exhibited distinct color banding at very low angles to the specimen axes (i.e., approximately vertical). These dark and light gray **anisotropies** reflect variations in impurity**content**[1]. Mineralogical data from BM **drillholes 107A, 107C, 108B** and **109B** reflect a halite content of at least **93%,** with anhydrite as the dominant impurity **(≤ 6%)**[1].

<u>West Hackberry</u> **(WH)**

West Hackberry dome is an irregularly shaped diapir located in Cameron Parish in southwestern Louisiana. The three **WH** test samples were from the depth interval **2290-2294** ft **(698.0-699.2** m) in **drillhole** 108. **Large** variations in grain sizes (range: c **.039-2.6** in; **<** 1-65 mm) **were** observed in all samples. No mineralogical data from these samples were available; however, these cores were the darkest of the **cores** tested, probably reflecting a higher concentration of impurities (perhaps up to **10%** anhydrite). There were no preferred orientations of grains or impurities noted.

EXPERIMENTAL TECHNIQUES

<u>Sample Preparation</u>

AU tests were performed on right circular cylinders. Raw cores were cut to an approximate length of 7.25-8.25 in **(18.4-21.0** cm) on a band saw, then experimental samples were machined to desired diameter (compression samples: **3.5**or 4.0 in (8.9 or 10 **cm);** extension samples: 3.5 in (8.9 cm)) and a length **of 7.0-8.0** in **(18-20** cm). The specimen **ends** were machined **flat** and parallel to witnin $\pm$ 0.001 in **($\pm$ .025** mm). The cores were turned using a tungsten carbide braze tool, Carboloy AX-~, Type 883. **By** using this technique, samples were obtained with sharp edges and minimal chipping or plucking of grains.

Prior to testing, all specimens were coated with a **.01-.02** in **(.25-.5** mm) thick layer of RTV **silastic** (RTV 108) to fill small surface pits. Each sample was then placed between vented steel end-caps and enclosed in a flexible jacket of Viton or Neoprene.

<u>Testing Apparatus and Procedures</u>

All mechanical tests were conducted **on** two identical triaxial apparatus[2] that are designed for quasi-static and creep experiments both in triaxial

compression $(\sigma_1 > \sigma_2 = \sigma_3)$ and trisxial extension $(\sigma_1 = \sigma_2 \, 7 \, \sigma_3)$. These machines are capable of testing samples of up to 4.0 in (10.8 cm) in diameter and 8.25 in (21.0 cm) in length, at confining pressures up to 10.0 kpsi (69.0 MPa) and temperatures up to 250°C.

Axial forces were generated by a cylindrical, hydraulic rsm, and measured by an external load cell. Fluidpressurewas applied using silicone fluid and was monitored with standard transducers. Axial deformation of the sample was determined with two diametrically opposed LVDT's (linear variable differential transformers), by subtracting out 'the calibrated system deformations within the active gauge length. .Lateral deformation was determined by means of one disk gauge[3] mounted at the central diameter along the specimen axis or measured dilatometrically. A detailed discussion of the techniques and data reduction procedures is given in an earlier report[4].

Once the samples were jacketed and placed in the vessel, the experimental sequence was initiated. For elevated temperature/pressure tests a hydrostatic confining pressure of 500 psi .(3.4 MPa) was applied to the sample while the sample-vessel system was heated. When the appropriate test temperature was reached, the fluid pressure was changed to the desired experimental level. The deviatoric stress loading was then started by increasing either (1) the axial stress in a compression test or (2) the fluid pressure in an extension test. The loading paths were not smooth ramps, but a series of fast (C2 sec) loading steps followed by four minutes of constant load. For every test, the initial stress increments were 250 psi (1.7 MPa). This loading technique resulted in an initial stress rate of 1.04 psi/sec (7.17 kpa/sec). Decreases in the stress rates of compression tests were caused by increases in specimen area with radial sample strain.

16

EXPERIMENTAL RESULTS

Test Conditions

The seventeen mechanical tests in this series included **triaxial** compression and extension experiments at mean stress rates of .66-1.04 psi/sec (4.5-7.2 kpa/sec), temperatures **from** 22 to 100°C and least principal stresses from 14.5 (atmospheric pressure) to 2000 psi (0.1 to 13.8 MPa). These ranges of pressures and temperatures were chosen since, under these conditions, **rocksalt** is pressure sensitive and prone to macroscopic failure. Table I is a matrix of experiments illustrating the specific sets of experimental conditions covered. The test/sample notation used in Table I and throughout this report consists of the following: dome, **drillhole** number/depth in feet **(meters)/test** type (C-compression, **E**-extension).

Test Data

The reader should note that the data presented in this report, and that referred to from earlier studies, **have** not been segregated by domal site. This procedure appeared justified because the scatter in the results of samples from different locations was within that observed for samples from the same location deformed under identical conditions.

The experimental data curves are presented in Figures 1 through 7. Example plots of deviatoric stress versus time and versus axial strain are given in Figures 1 and **2A,** respectively. The first graph illustrates the stepped loading path used in this test series. Figures **2B-7** are plots involving a combination of differential stress, differential strain and/or volumetric strain. The graphs have been chosen to exemplify (1) reproducibility of results (Figure **2**), (2) effect of σ_3 changes in compression (Figures 3 and **4**), (3) effect of σ_3 and T changes in compression

Table I

Matrix of Experiments

Least Principal Stress (psi/MPa)	Temperature (°C)		
	22	60	100
14.5/0.10	BC 19A/2581(786.7)/C BM 110A/2688.5(819.4)/C BM 110B/3724(1135.0)/C	WH 108/2294(699.2)/C	BM 110B/3728(1136.2)/C
250/1.72	BM 110A/2687(819.0)/C BM 110A/2691(820.2)/E		
500/3.45	BM 107C/2512(765.6)/E	BC 19A/2579(786.0)/E WH 108/2291(698.3)/C	BM 110A/2685(818.3)/C BM 110B/3723(1134.7)/C
1500/10.3	BM 110A/2692(820.5)/C BM 110B/3726(1135.6)/E		BM 110A/2683.5(817.9)/C
2000/13.8		BC 19A/2576(785.1)/E WH 108/2290(698.0)/C	

(Figure 5), (4) effect of σ_3 changes in extension (Figure 6) and (5) comparison of compression and extension at constant σ_3 and T (Figure 7). Test data at maximum differential stresses and the elastic constants are summarized in Tables II and III, respectively. Six samples tested did not reach ultimate strength (see Table II), and therefore the maximum value is given. The maximum differential stresses reported are the absolute peak stresses attained throughout the stepped loading history of each sample. The maximum strains correspond directly to the values at the maxmium differential stress.

The summary plots in Figures 8-11 illustrate the effects of σ_3 and T on differential stress and axial strain (i.e., greatest principal strain) in compression and extension. As noted on the graphs, most of the data points plotted are actual ultimate stresses and axial strains at failure. The maximum data are included for completeness, but are only lower bounds on the appropriate ultimate stresses and strains.

The experimental results presented here are consistent in trends and magnitudes with other published rocksalt data, including two earlier reports on domal rocksalt[596]. As shown in Figures 8 and 9, rocksalt is pressure sensitive in the 14.5-2000 psi (0.1-13.8 MPa) range. As expected, within the range of σ_3 values salt becomes distinctly stronger with increased least principal stress. Ductility (greatest principal strain to failure) is also directly related to σ_3, The effect of temperature on strength and ductility is shown in Figures 10 and 11. At atmospheric pressure, no trend of temperature dependence on strength is seen, while ductility increases slightly with temperature. However, at higher pressures (500 psi; 3.45 MPa and 1500 psi; 10.3 MPa), strength decreases with increasing temperature. In compression, ductility increases with temperature,

Table II

Test Data at **Maximum** Deviatoric Stress

Test Sample Drillhole/Depth-Ft(m)/ Test Type	σ_3 psi(MPa)	T °C	$(\sigma_1 - \sigma_3)_m$ kpsi(MPa)	$(e_1)_m$ %	$(-e_3)_m$ %	$(e_1 - e_3)_m$ %	$(e)_m$ %
BC 19A/2581(786.7)/C	14.5(0.1)	22	3.74(25.8)*	3.01	3.12	6.14	-3.24
BM 110A/2688.5(819.4)/C	14.5(0.1)	22	2.81(19.4)*	2.02	3.00	5.02	-3.99
BM 110B/3724(1135.0)/C	14.5(0.1)	22	4.02(27.7)*	3.10	4.51	7.60	-5.91
BM 110A/2687(819.0)/C	250(1.72)	22	6.05(41.7)*	7.49	5.56	13.1	-3.62
BM 110A/2692(820.5)/C	1500(10.3)	22	9.54(65.8)*	31.3	18.2	49.5	-5.10
WH 108/2294(699.2)/C	14.5(0.1)	60	3.79(26.1)*	4.27	4.47	8.74	-4.66
WH 108/2291(698.3)/C	500(3.45)	60	5.78(39.9)*	18.8	11.5	30.3	-4.22
WH 108/2290(698.0)/C	2000(13.8)	60	7.50(51.7)	23.8	13.0	36.8	-2.24'
BM 110B/3728(1136.2)/C	14.5(0.1)	100	3.74(25.8)*	4.45	5.62	10.1	-6.78
BM 110A/2685(818.3)/C	500(3.45)	100	5.32(36.7)*	23.6	15.2	38.9	-6.77
BM 110B/3723(1134.7)/C	500(3.45)	100	5.46(37.7)*	23.2	14.1	37.3	-5.12
BM 110A/2683.5(817.9)/C	1500(10.3)	100	6.54(45.1)	32.4	18.3	50.7	-4.80
BM 110A/2691(820.2)/E	250(1.72)	22	6.62(45.7)	3.54	8.67	12.2	-1.59
BM 107C/2512(765.6)/E	500(3.45)	22	7.43(51.2)*	5.22	9.61	14.8	0.830
BM 110B/3726(1135.6)/E	1500(10.3)	22	8.46(58.3)	6.27	12.1	18.4	0.421
BC 19A/2579(786.0)/E	500(3.45)	60	4.98(34.3)	3.49	7.29	10.8	-0.305
BC 19A/2576(785.1)/E	2000(13.8)	60	6.44(44.4)	6.65	11.9	18.5	1.46

it Actual ultimate stress value.

Table III

Elastic (Unloading) Constants

Test Sample Drillhole/Depth-Ft(m)/ Test Type	σ_3 psi(MPa)	T °C	E^a Mpsi(GPa)	ν^a	G^b Mpsi(GPa)	K^b Mpsi(GPa)
BM 110A/2687(819.0)/C	250(1.72)	22	4.57(31.5)	.27	1.80(12.4)	3.31(22.8)
BM 110A/2692(820.5)/C	1500(10.3)	22	5.36(37.0)	.31	2.05(14.1)	4.70(32.5)
WH 108/2291(698.3)/C	500(3.45)	60	5.37(37.0)	.32	2.03(14.0)	4.97(34.3)
WH 108/2290(698.0)/C	2000(13.8)	60	5.68(39.2)	.23	2.31(15.9)	3.51(24.2)
BM 110A/2685(818.3)/C	500(3.45)	100	4.57(31.5)	.28	1.79(12.3)	3.46(23.9)
BM 110B/3723(1134.7)/C	500(3.45)	100	4.92(33.9)	.28	1.92(13.2)	3.73(25.7)
BM 110A/2683.5(817.9)/C	1500(10.3)	100	4.11(28.3)	.39	1.48(10.2)	6.23(42.9)
BM 107C/2512(765.6)/E	500(3.45)	22	4.91(33.9)	.33	1.85(12.7)	4.81(33.2)

[a] measured

[b] calculated

as has been previously published. Equivalent data for extension are less complete. The ultimate differential stresses were reached in only two of four experiments; however, the same trend of decreasing strength and increasing ductility with temperature is suggested. Volumetric strain measurements are also influenced by least principal **stress** and temperature (see Table II). Dilatancy at fixed values of principal stress difference decreases as pressure and/or temperature **is raised.**

As an earlier report[6] discussed, there are marked differences between compression and extension results from tests at equivalent T and σ_3. In general, the extension samples are approximately the same **strength,** but reach **far** less greatest principal, differential and volumetric strains at failure than the compression samples. These contrasting results are attributed to distinctly different failure modes. All extension samples taken to **failure broke** suddenly along a single extension fracture (i.e., a fracture perpendicular to σ_3); whereas, the compression specimens tended to fail more stably by the formation of many mesoscopic **(.5-3.0** in; **1.3-7.6** cm) shear and extension cracks preceding the loss of cohesion on one or more macroscopic shear fractures. The volumetric strain data presented here and from the two previous studies should prove to be significant in **the development** of a general fracture criterion for rocksalt.

The elastic (unloading) constants obtained in this test series are presented in Table III. The Young's moduli and Poisson's ratios fall within the ranges of values previously published. These experimentally measured values were used to calculate the shear and bulk moduli. By combining these data with those from two earlierreports[5,6], mean elastic constants were determined for Bryan Mound, West Hackberry and overall **SPR rocksalt** (Table IV). The stated value of E is 18 percent higher for West

22

Table IV

Mean Elastic Constants[a]

Location	K[c] Mpsi (GPa)	ν[b]	G[c] Mpsi (GPa)	
Bryan Mound	4.72 (32.6)	.33	1.77 (12.2)	4.63 (31.9)
West Hackberry	5.57 (38.4)	.30	2.14 (14.8)	4.64 (32.0)
Overall	4.94 (34.1)	.32	1.87 (12.9)	4.57 (31.5)

[a] Data from references 5 and 6 and this report.

[b] Mean of measured values.

[c] Calculated from E and v values.

Hackberry than for **Bryan** Mound. This result may be due to West Hackberry ssmples containing a greater concentration of impurities (e.g., anhydrite) **than** the Bryan Mound material.

SUMMARY AND CONCLUSIONS

Seventeen quasi-static experiments on **rocksalt** from three SPR sites have been presented. **The** test results were reproducible and consistent with previously published data. The minor variations in sample grain sizes and in composition did not appear to have an effect on strength and behavior trends. As expected, specimen strength was directly related to the least principal stress and inversely related to temperature; further-more, pressure and temperature increases resulted in larger axial strains to failure (ductility). While strengths in extension and compression were similar, ultimate strains were substantially higher in compression than in extension.

REFERENCES

1. Bild, R. W. (1980), "Chemistry and Mineralogy of Samples from the Strategic Petroleum Reserve Bryan Mound Site," Sandia National Laboratories Report, SAND80-1258, Sandia National Laboratories, Albuquerque, NM, 50 p.

2. Wawersik, W. R. and D. W. Hannum (1980), "Mechanical Behavior of New Mexico Rock Salt in Triaxial Compression up to $200^\circ C$," J. Geophys. Res., 85, B2, 891-900.

3. Schuler, K. W. (1978), "Lateral Deformation Gauge for Rock Mechanics Testing," Exp. Mech., 18, 12.

4. Wawersik, W. R. (1979), "Indirect Deformation (Strain) Measurements and Calibrations in Sandia Triaxial Apparatus for Testing to $250^\circ C$," Sandia National Laboratories Report, SAND79-0114, Sandia National Laboratories, Albuquerque, NM, 44 p.

5. Wawersik, W. R., D. W. Hannum and H. S. Lauson (1980), "Compression and Extension Data for Dome Salt from West Hackberry, Louisiana," Sandia National Laboratories Report, SAND79-0668, Sandia National Laboratories, Albuquerque, NM, 34 p.

6. Wawersik, W. R., D. J. Holcomb, D. W. Hannum and H. S. Lauson (1980), "Quasi-Static and Creep Data for Dome Salt from Bryan Mound, Texas," Sandia National Laboratories Report, SAND80-1434, Sandia National Laboratories, Albuquerque, NM, 36 p.
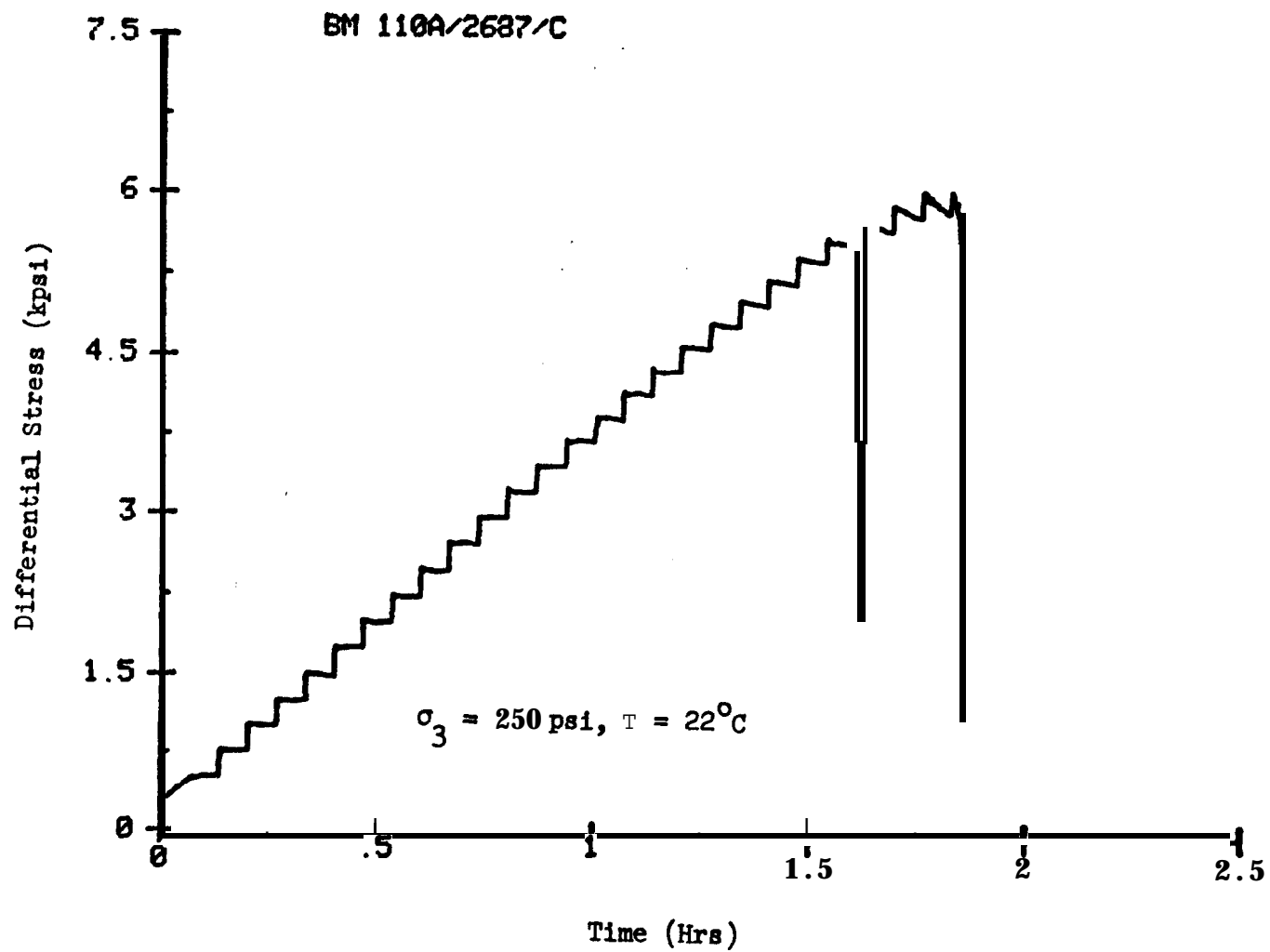
Figure 1: Differential stress-time curve for sample BM 110A/2687 deformed in compression at 250 psi and 22°C
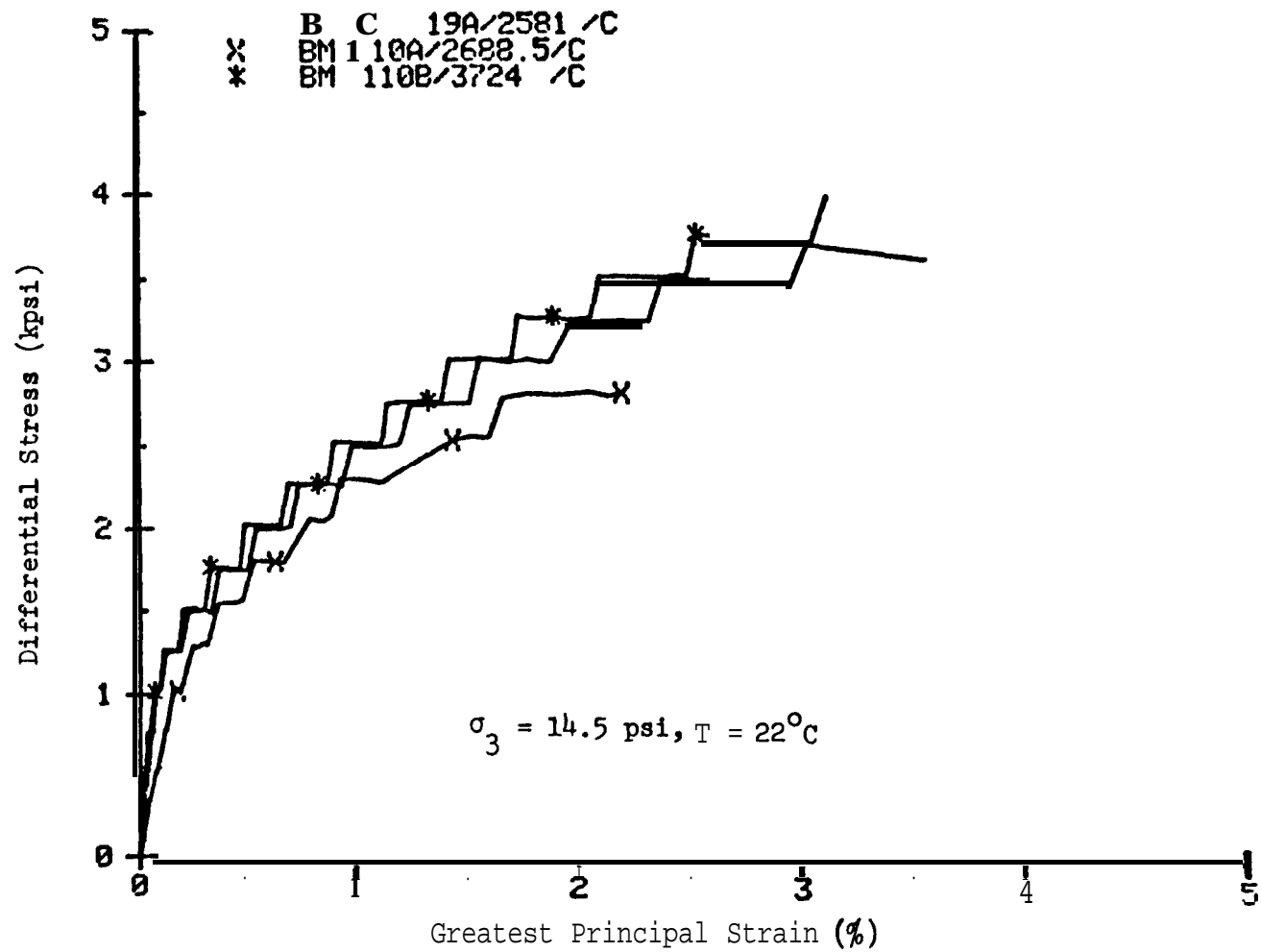
Figure 2A: Differential stress-greatest principal strain curves for samples BC 19A/2581, BM 110A/2688.5 and BM 110B/3724 deformed in compression at 14.5 psi and 22°C.
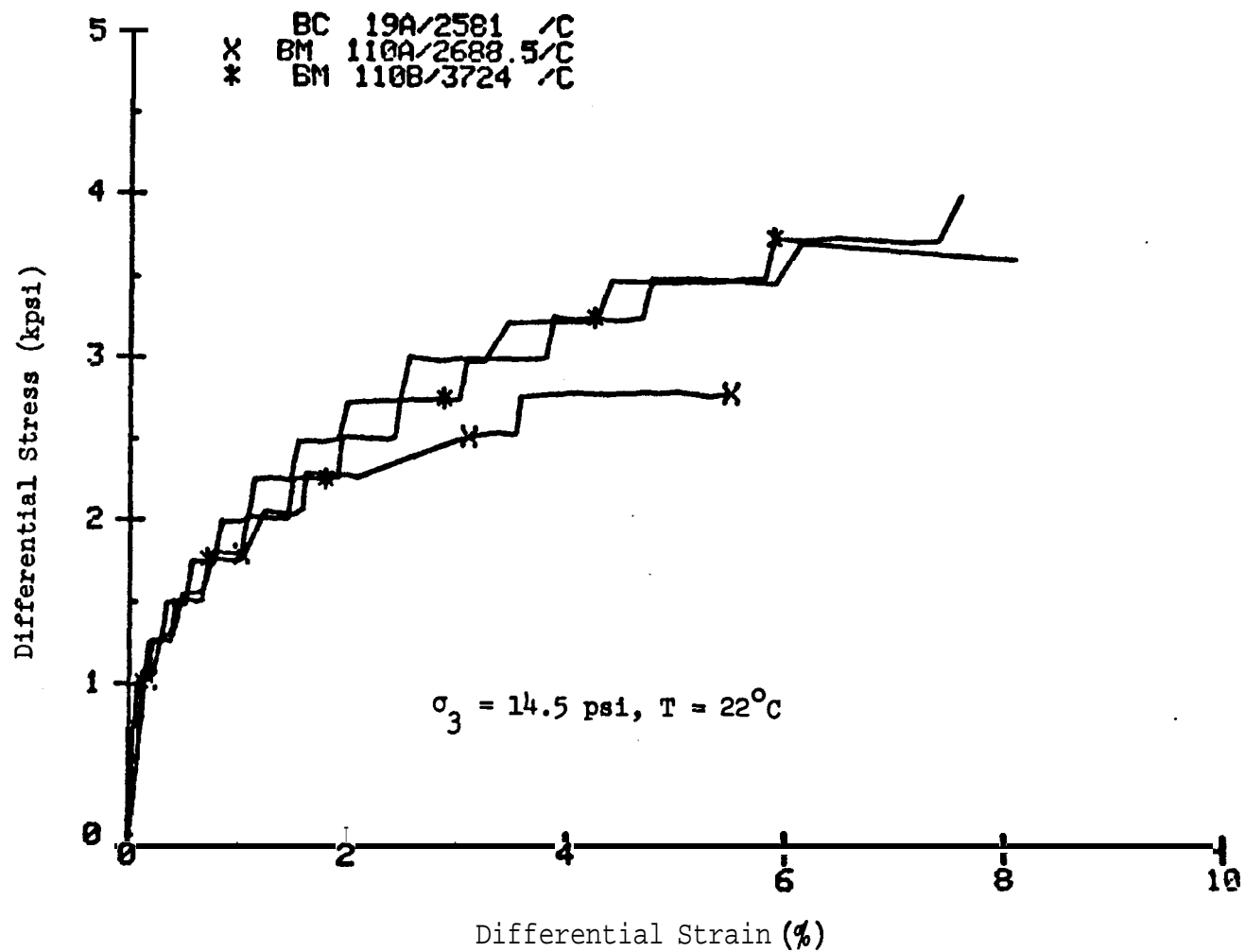
Figure 2B: Differential stress-differential strain curves for samples BC 19A/2581, BM 110A/2688.5 and BM 110B/3724 deformed in compression at 14.5 psi and 22°C.
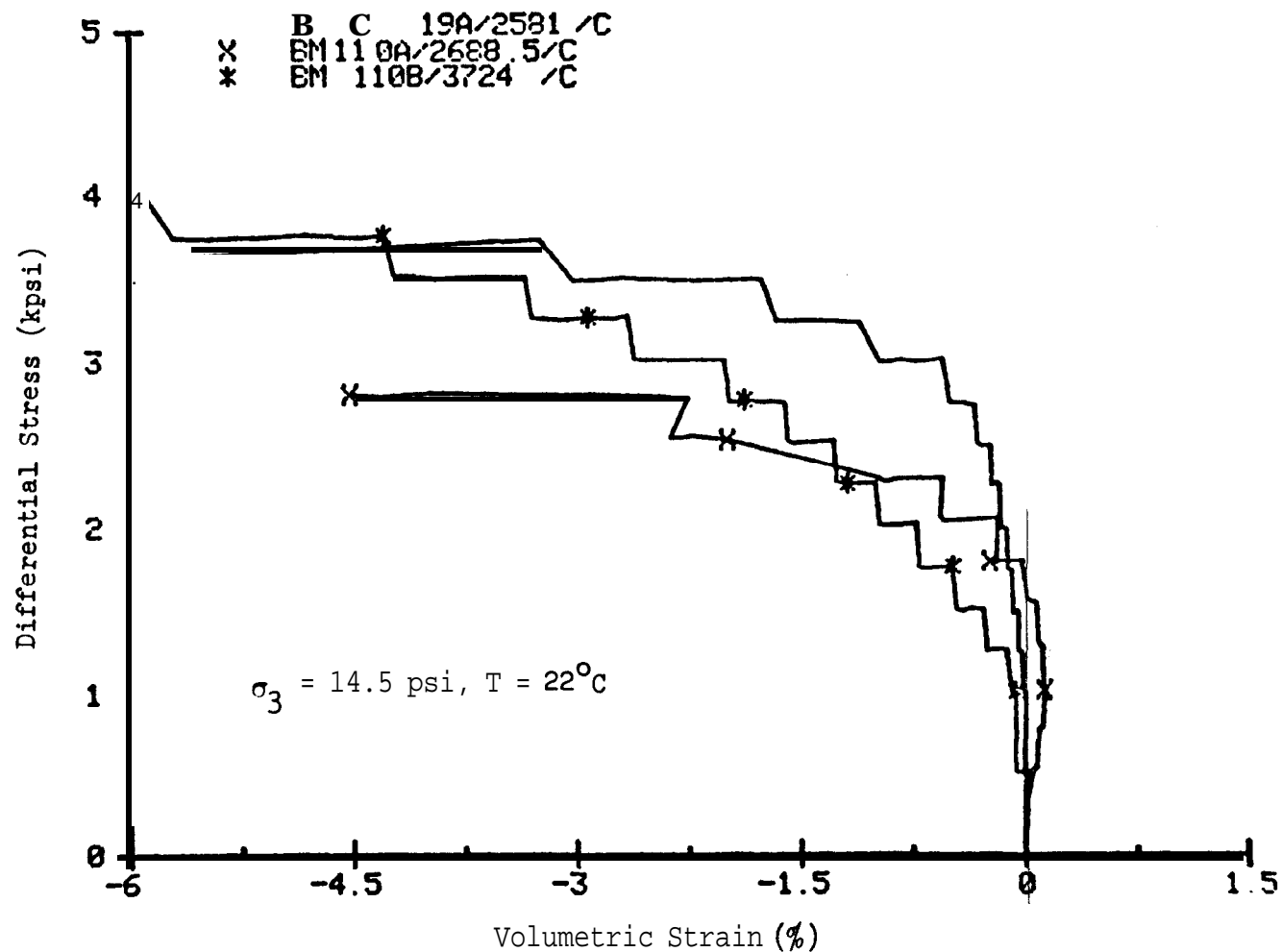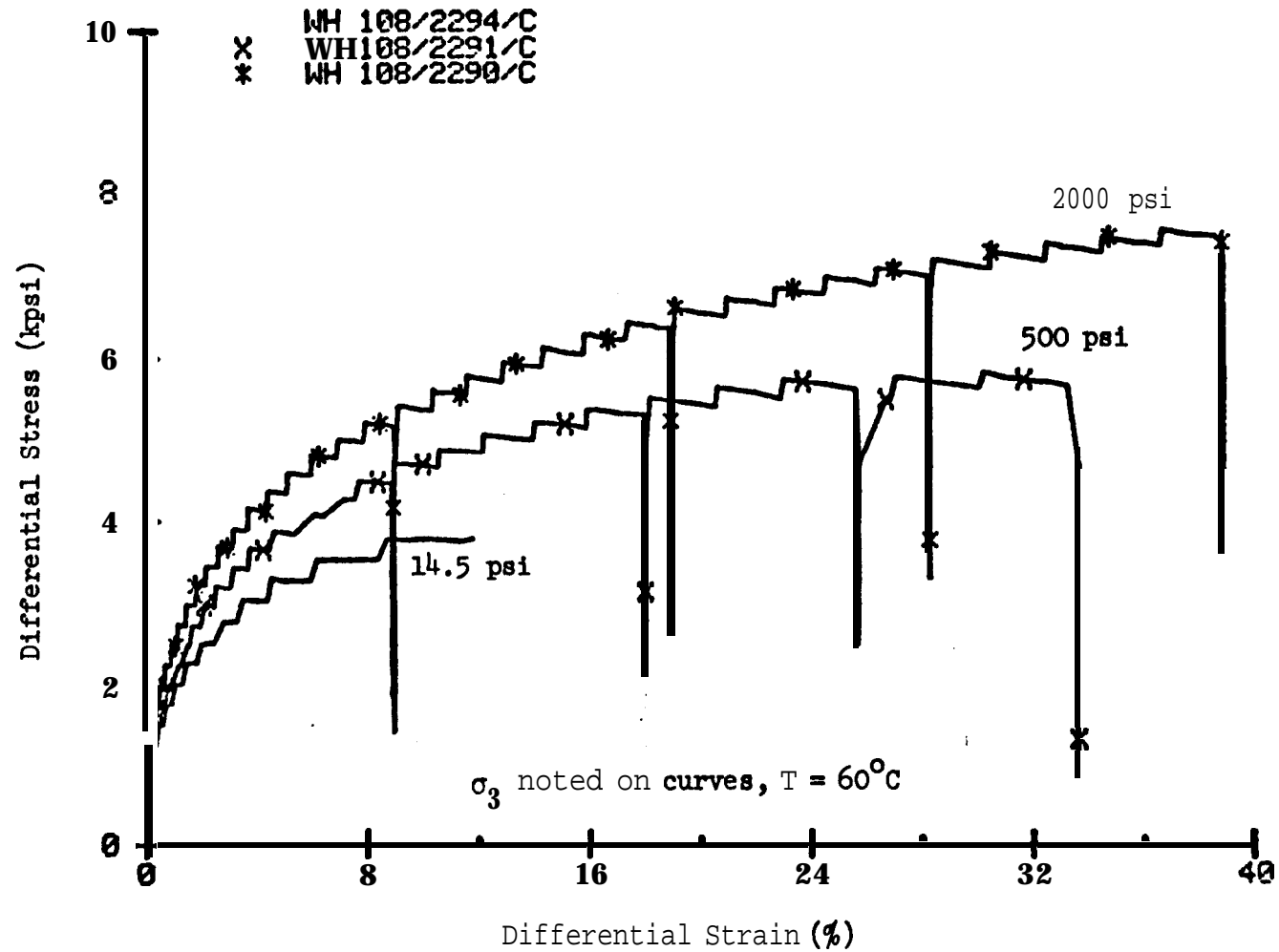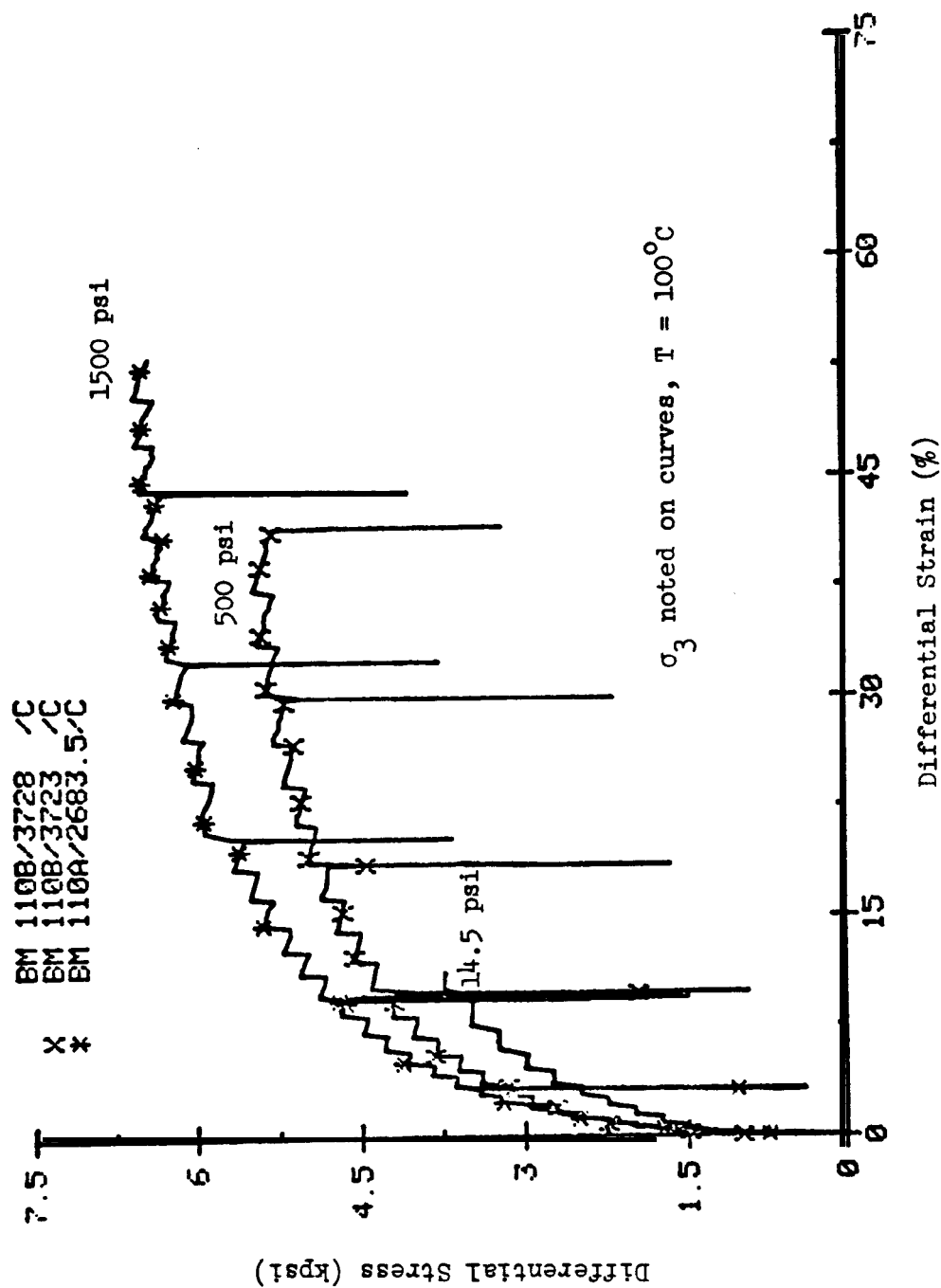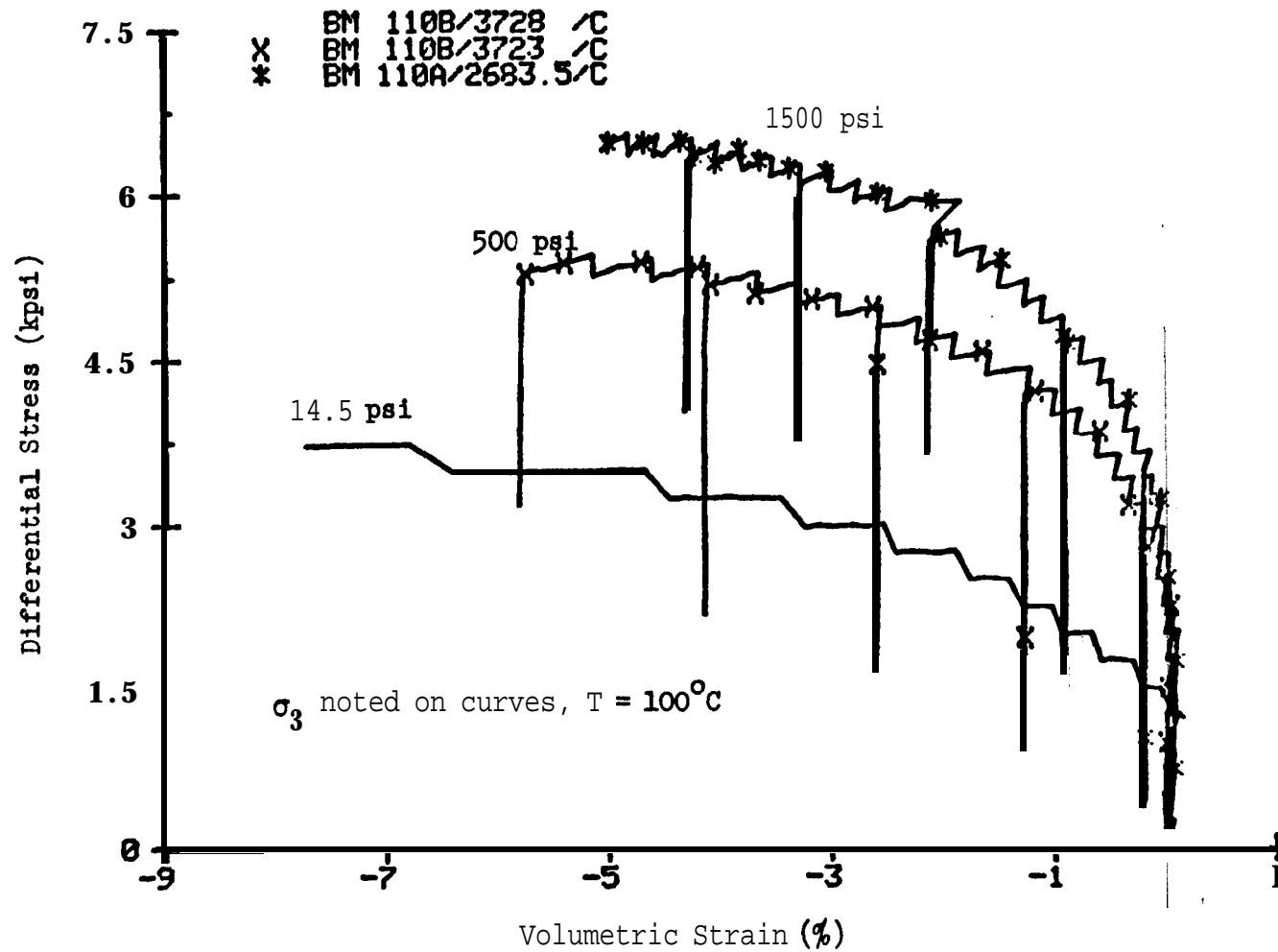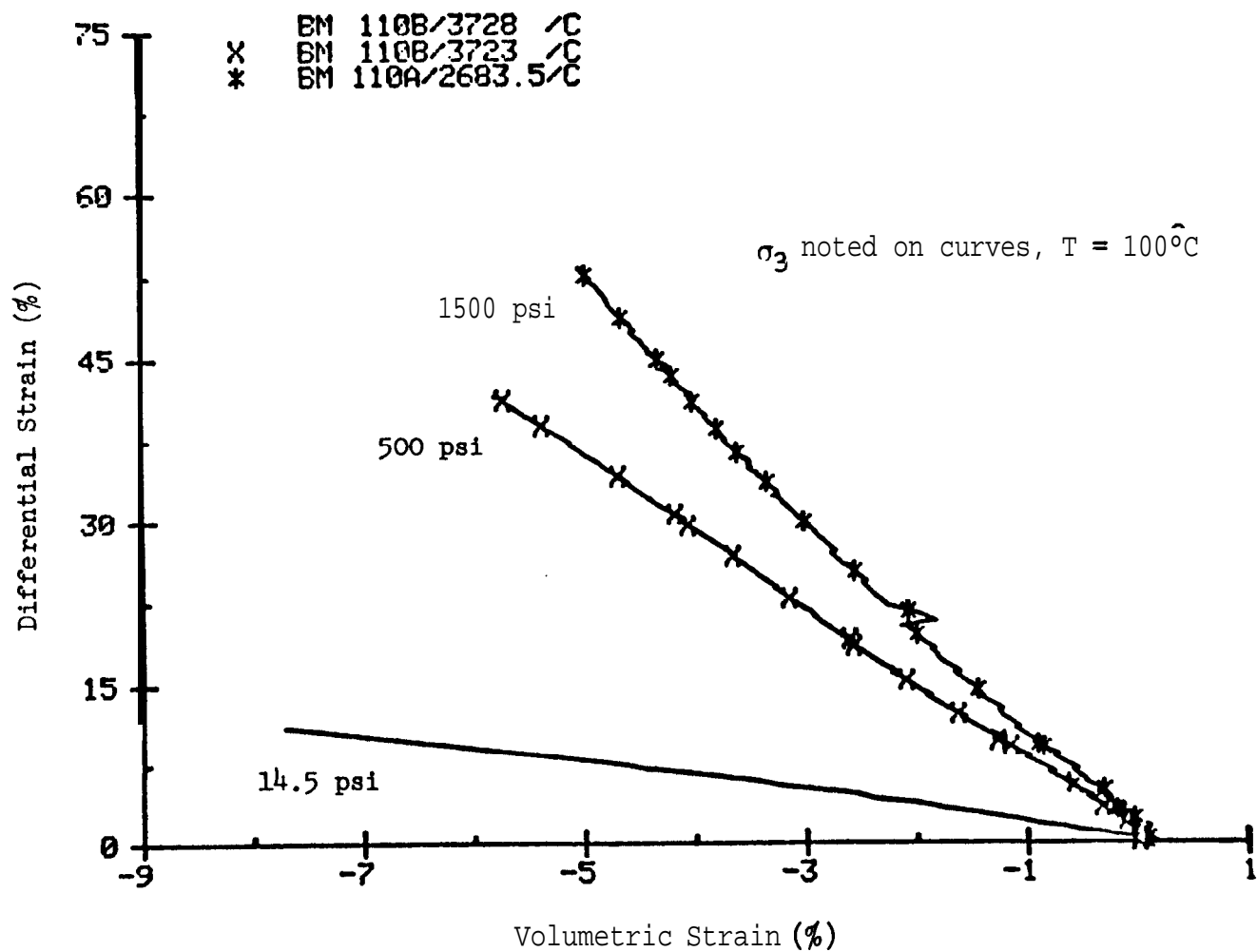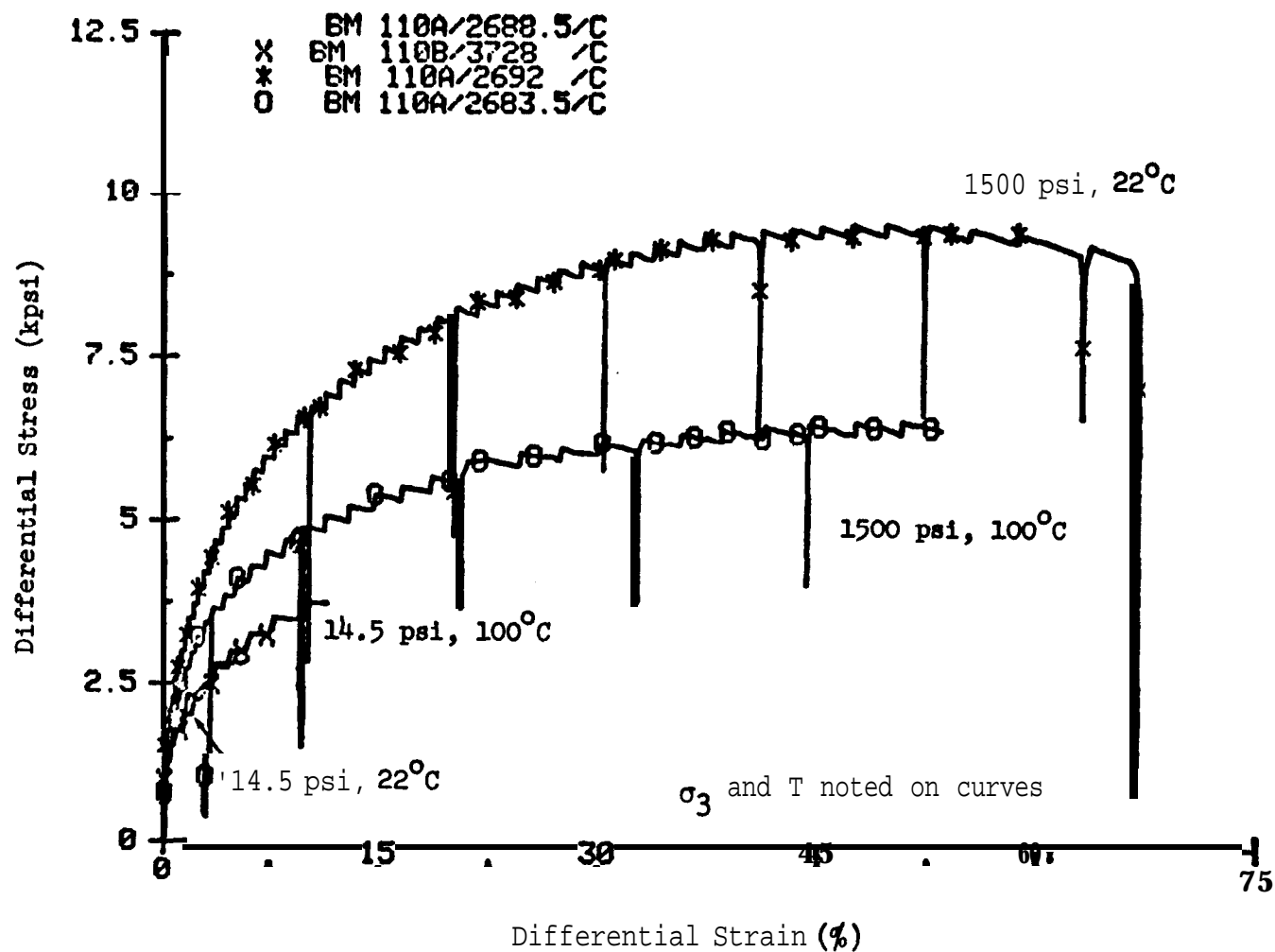
Figure 2C: Differential stress-volumetric strain curves for samples BC 19A/2581, BM 110A/2688.5 and BM 110B/3724 deformed in compression at 14.5psi and 22°C.

Figure 3A: Differential stress-differential strain curves for samples WH 108/2294, WH 108/2291 and WH 108/2290 deformed in compression at 14.5, 500, 2000 psi and 60°C.
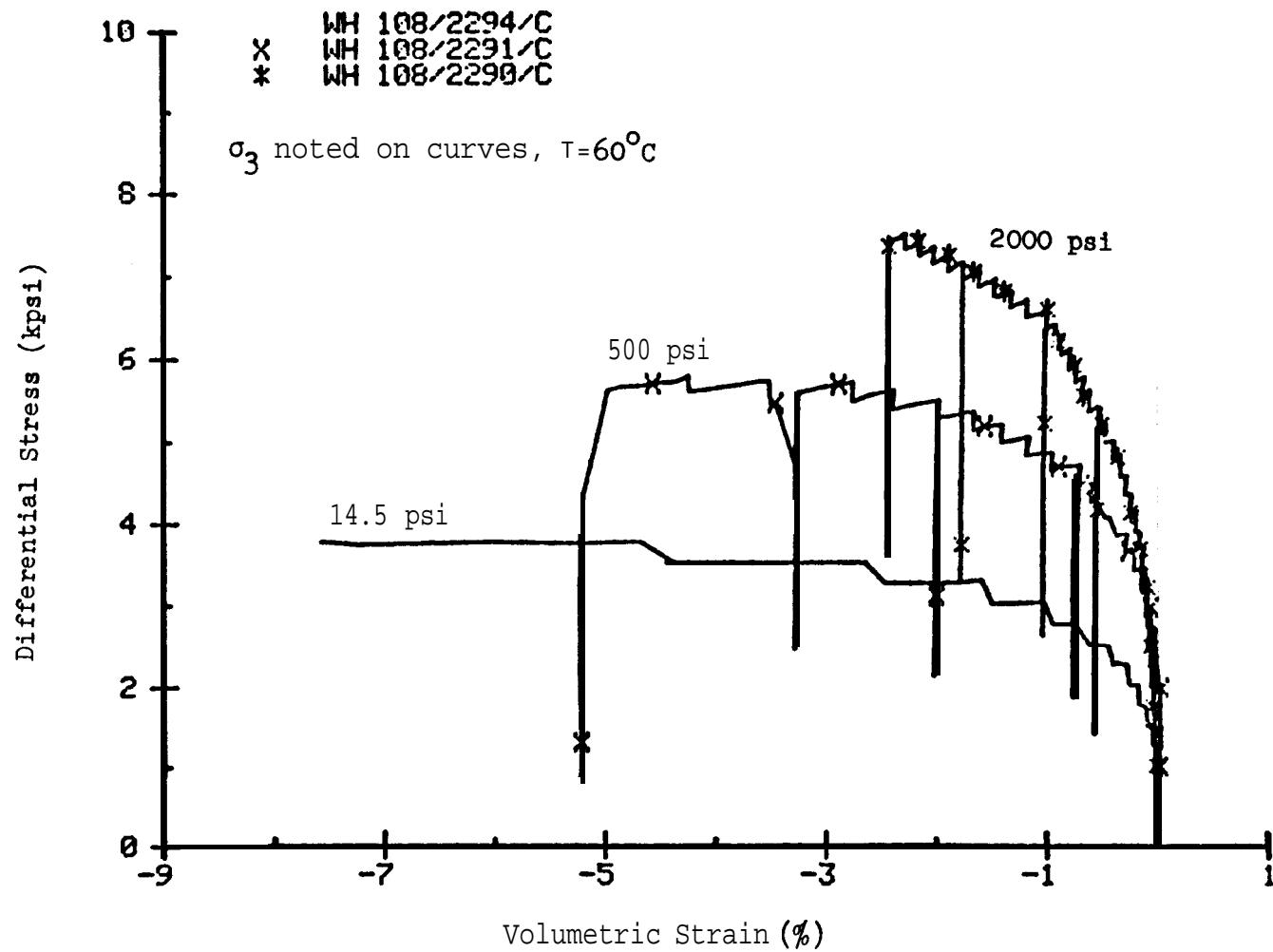
Figure 3B: Differential stress-volumetric strain curves for samples WH 108/2294, WH 108/2291 and WH 108/2290 deformed in compression at 14.5, 500, 2000 psi and 60°C.
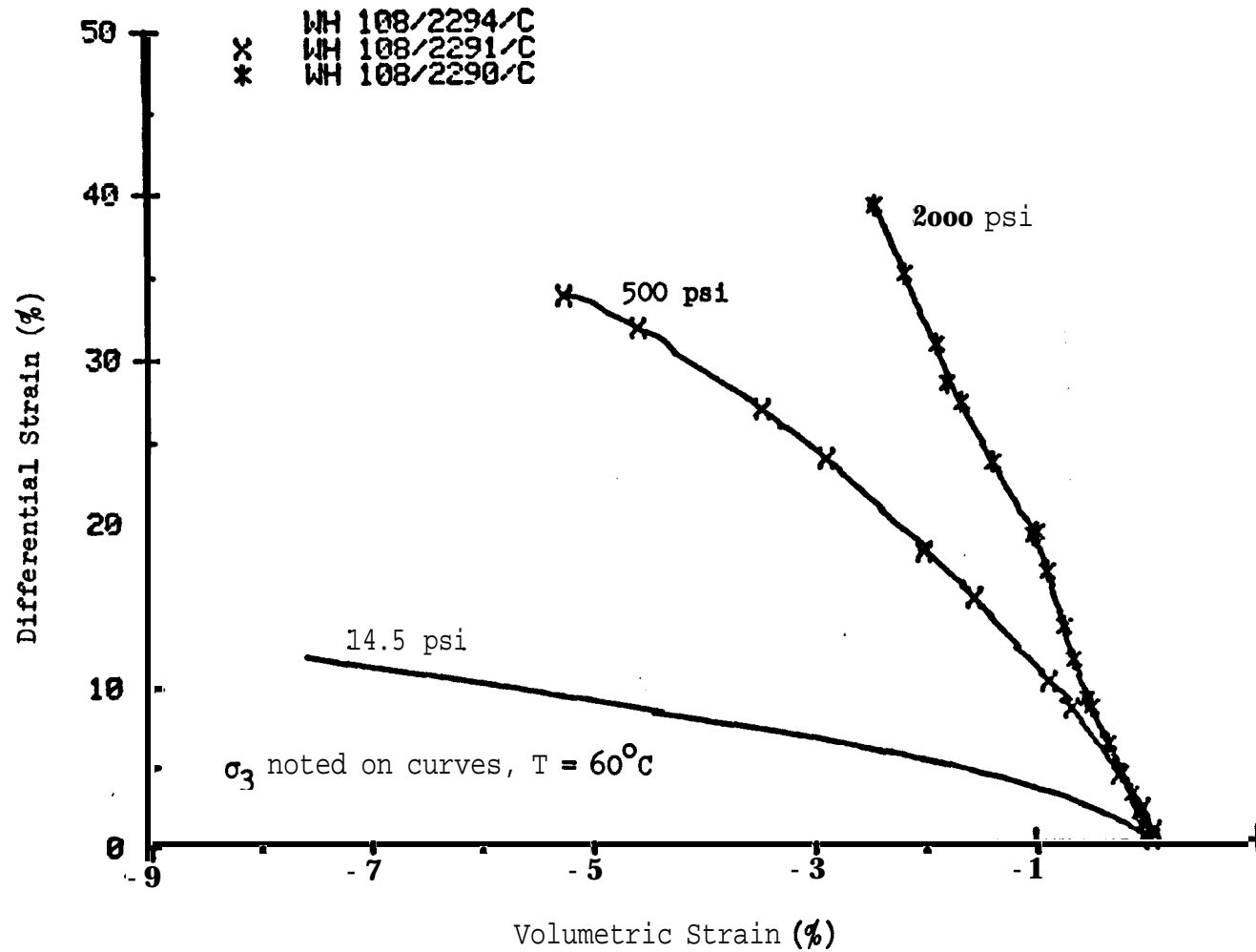
Figure 3C: Differential strain-volumetric strain curves for samples WH **108/2294,** WH **108/2291** and WH **108/2290** deformed in compression at 14.5, 500, 2000 psi and **60°C.**

Figure 4A: Differential stress-differential strain curves for samples BM 110B/3728, BM 110B/3723 and BM 110A/2683.5 deformed in compression at 14.5, 500, 1500 psi and 100°C.

Figure 4B: Differential stress-volumetric strain curves for samples BM 110B/3728, BM 110B/3723 and BM 110A/2683.5 deformed in compression at 14.5, 500, 1500 psi and 100°C.

Figure 4C: Differential strain-volumetric strain curves for samples BM 110B/3728, BM 110B/3723 and BM110A/2683.5 deformed in compression at 14.5, 500, 1500 psi and 100°C.

Figure 5A: Differential stress-differential strain curves for samples BM 110A/2688.5 and BM 110B/3728 deformed in compression at 14.5 psi and 22, 100°C; and BM 110A/2692 and BM 110A/2683.5 deformed in compression at 1500 psi and 22, 100°C.
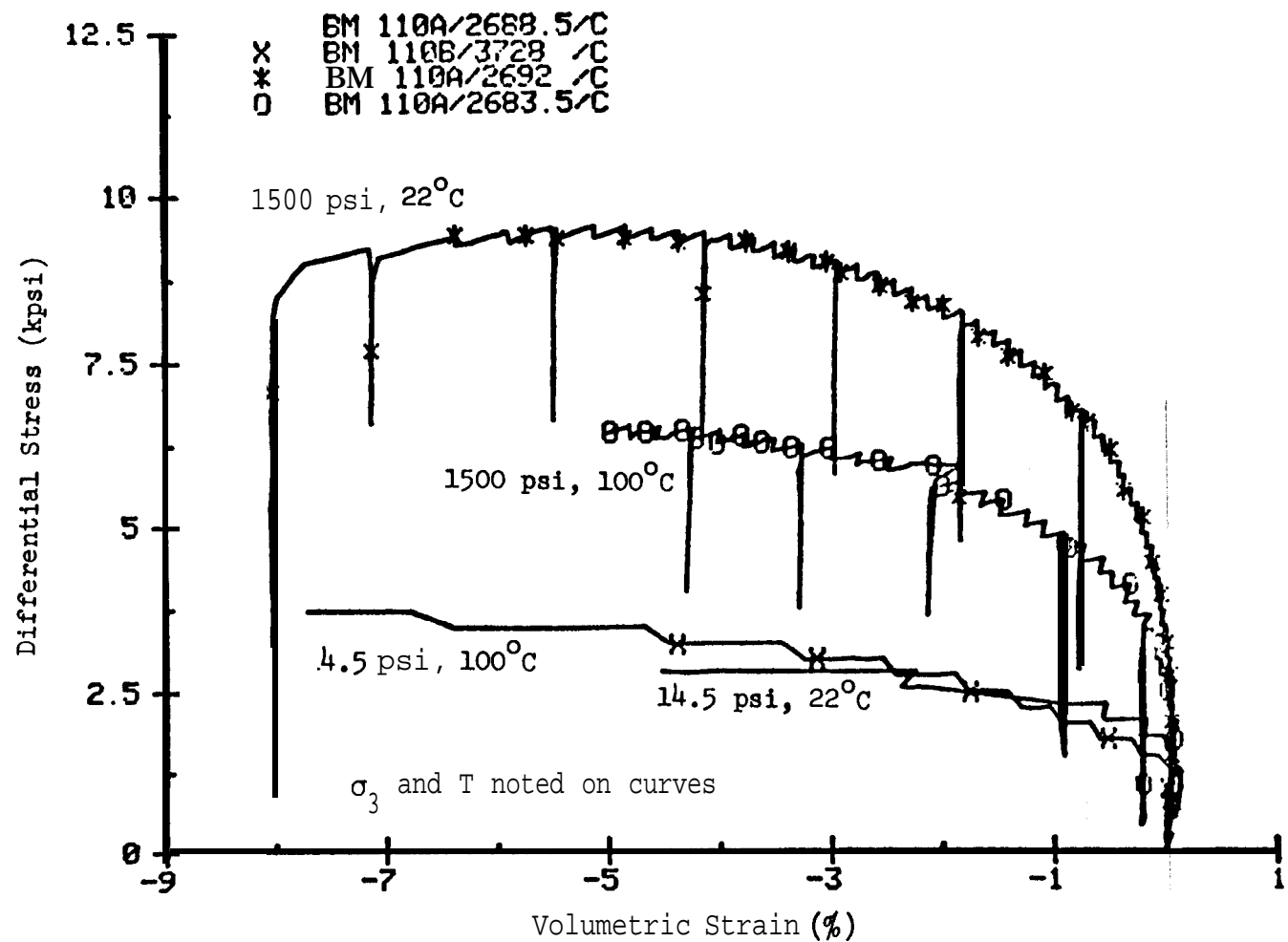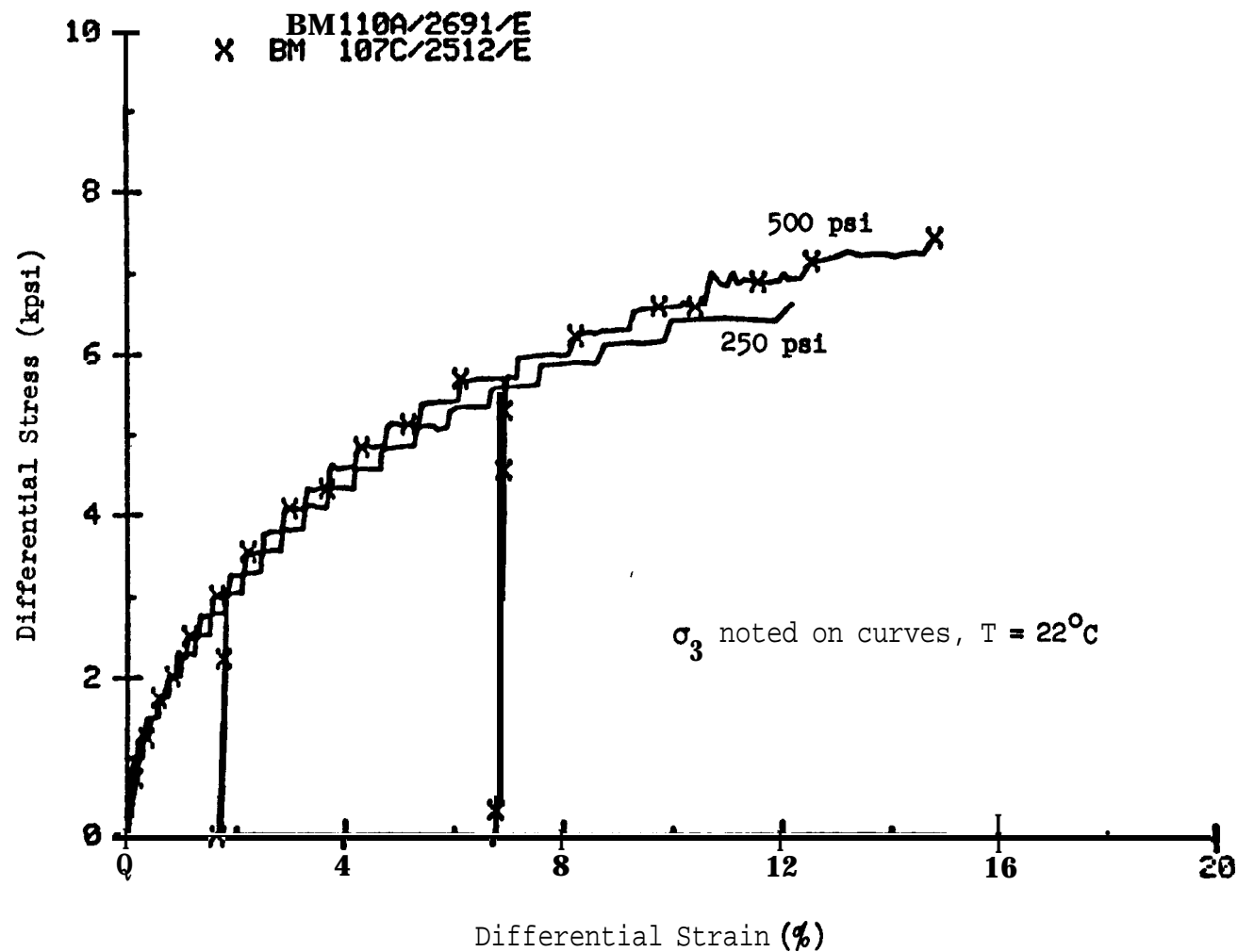
Figure 5B: Differential stress-volumetric strain curves for samples BM 110A/2688.5 and BM 110B/3728 deformed in compression at 14.5 psi and 22, 100°C; and BM 110A/2692 and BM 110A/2683.5 deformed in compression at 1500 psi and 22, 100°C.

Figure 6A: Differential stress-differential strain curves for samples BM 110A/2691 and BM 107C/2512 deformed in extension at 250, 500 psi and 22°C.
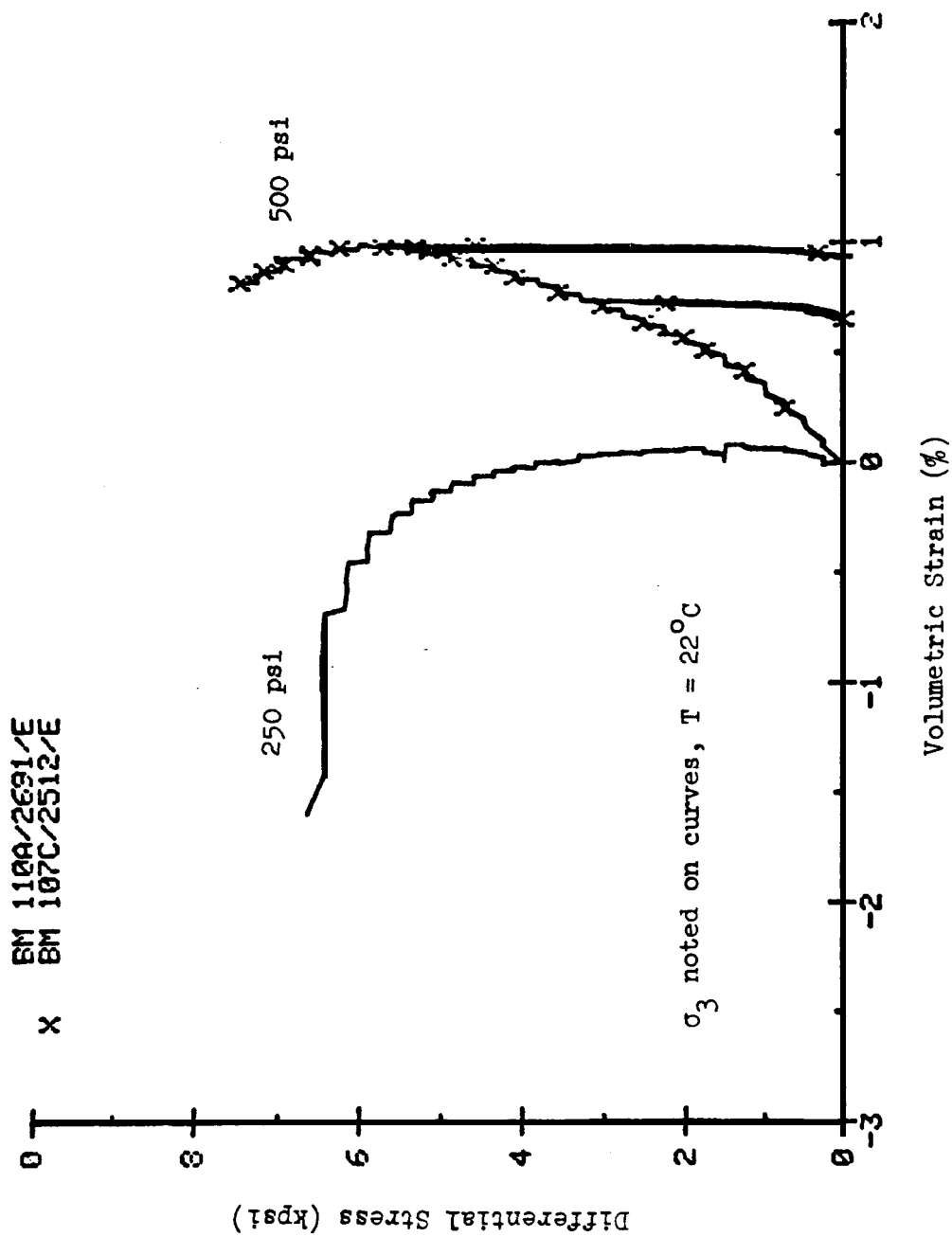
Figure 6B: Differential stress-volumetric strain curves for samples BM 110A/2691 and BM 107C/2512 deformed in extension at 250, 500 psi and 22°C.
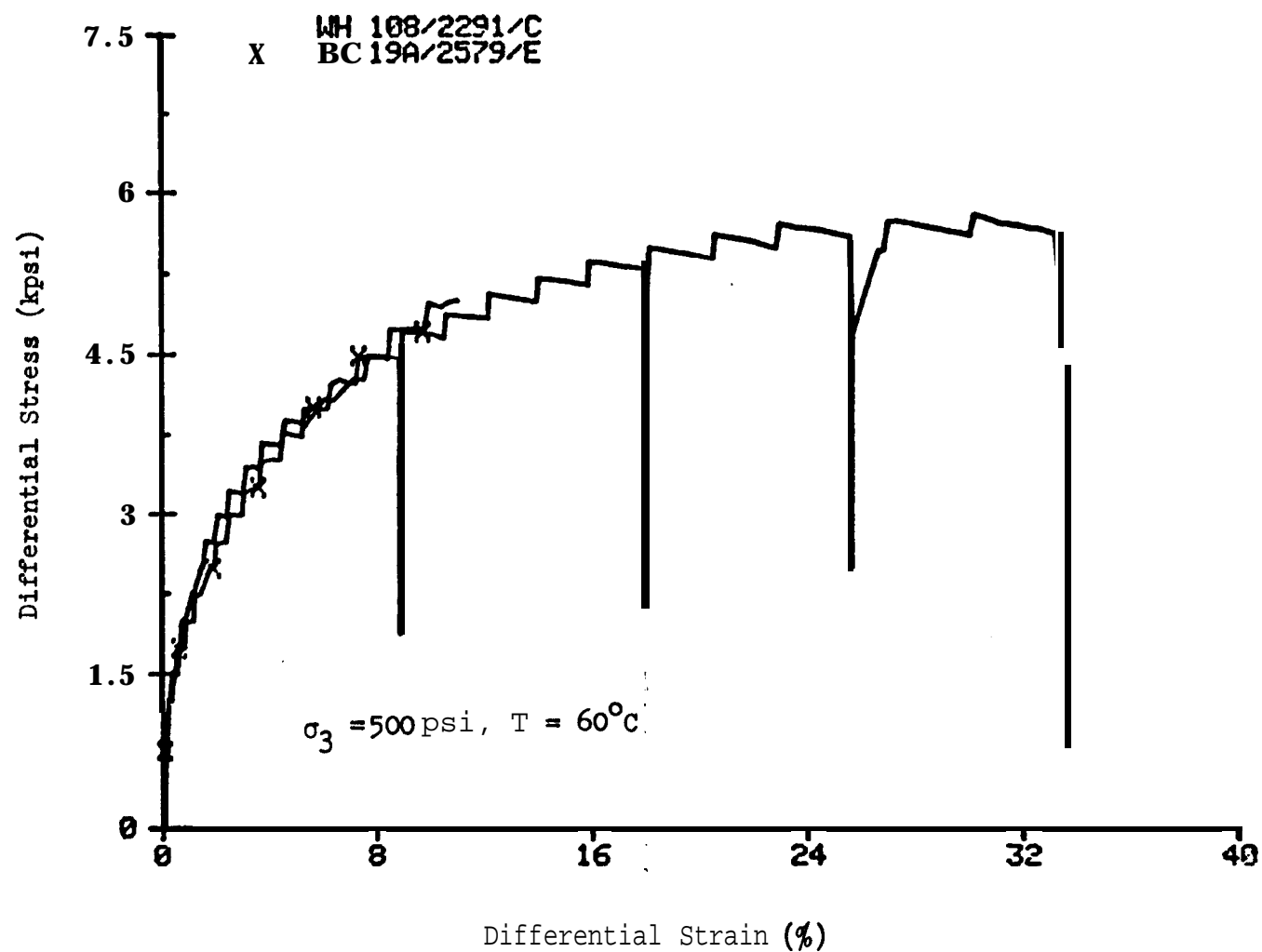
Figure 7A: Differential stress-differential strain curves for sample WH 108/2291 deformed in compression and BC 19A/2579 deformed in extension at 500 psi and 60°C.
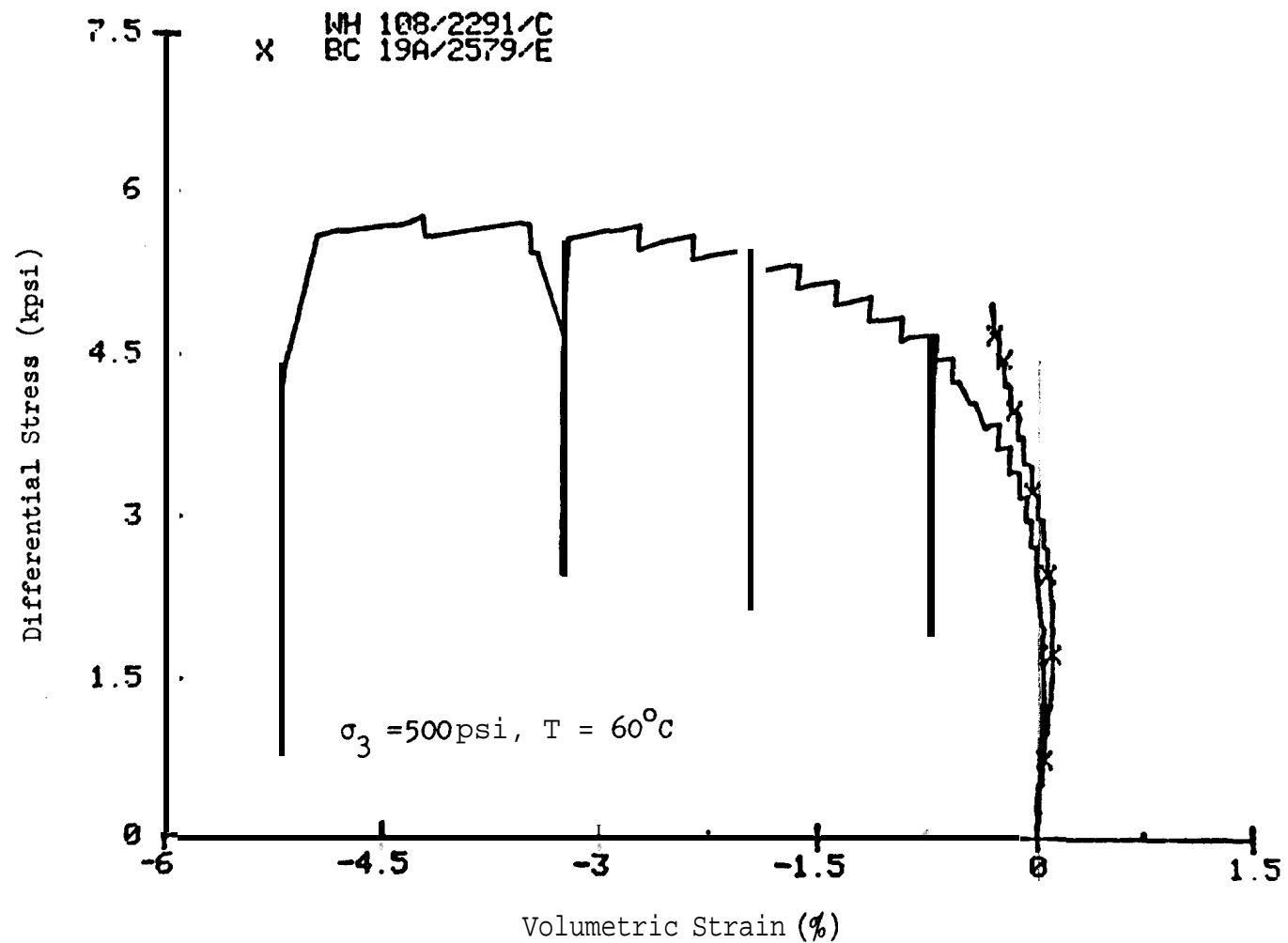
Figure 7B: Differential stress-volumetric strain curves for sample WH 108/2291 deformed in compression and BC 19A/2579 deformed in extension at 500 psi and 60°C.
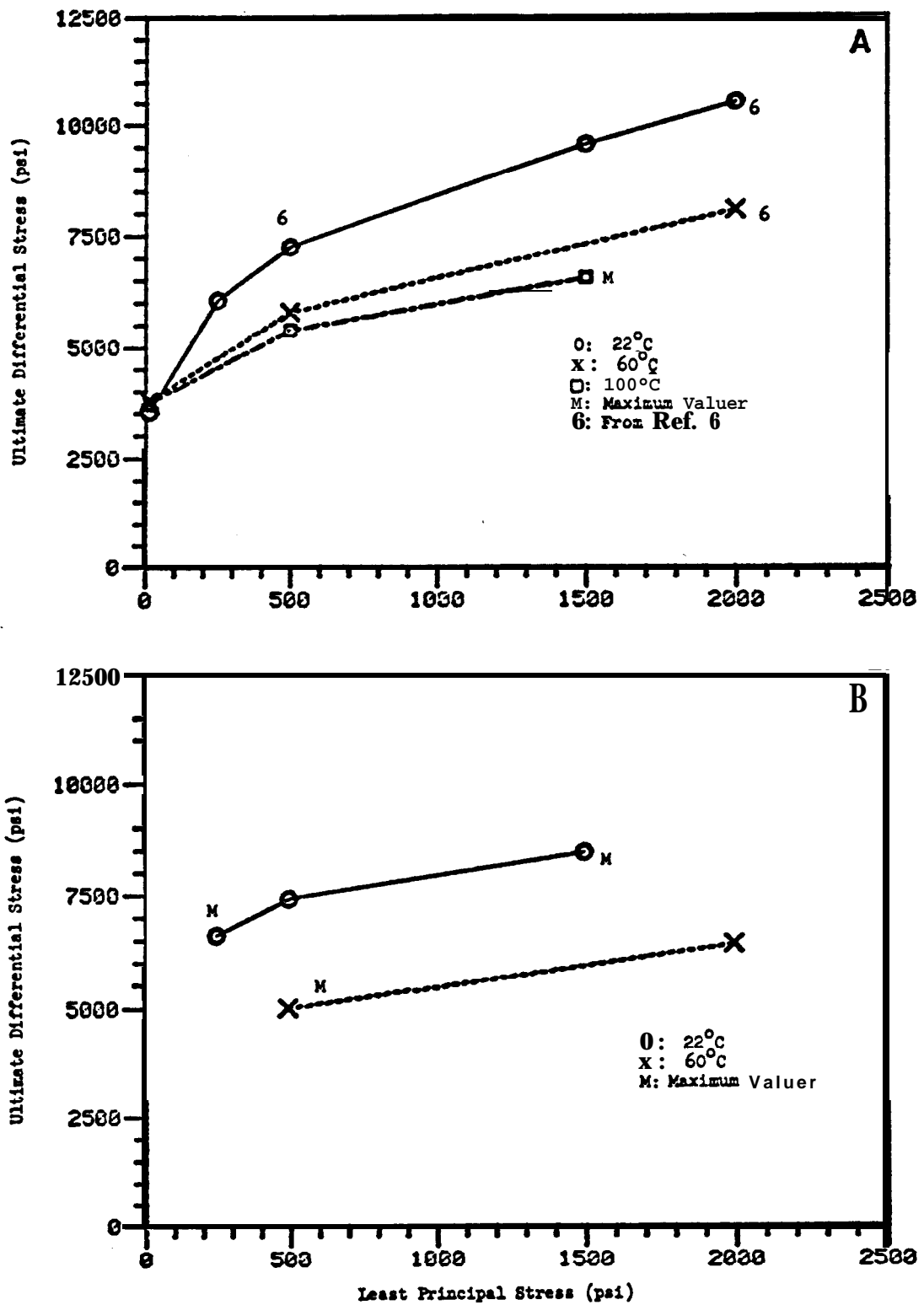
Figure 8: Ultimate differential stress-least principal stress plots for samples deformed in (A) compression and (B) extension.
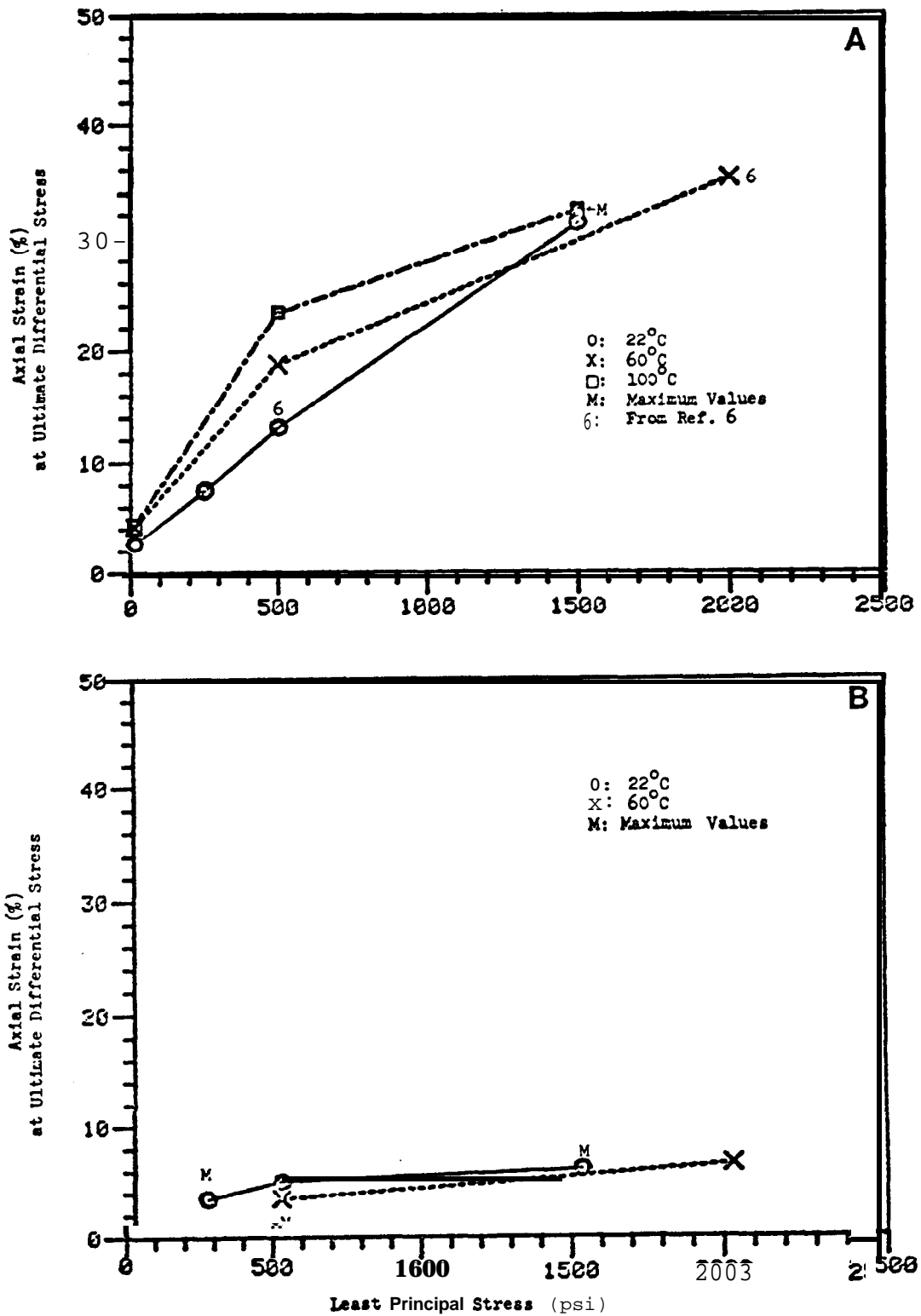
Figure 9: Axial strain at $(\sigma_1 - \sigma_3)_u$-least principal stress plots for samples deformed in (A) compression and (B) extension.
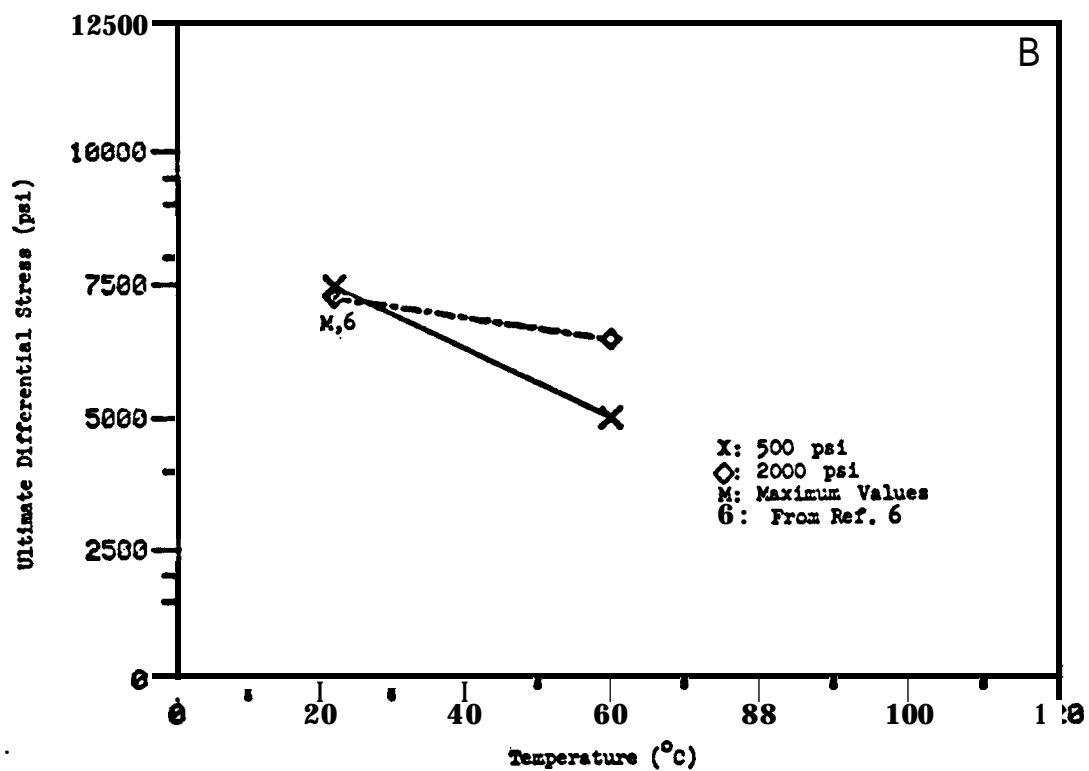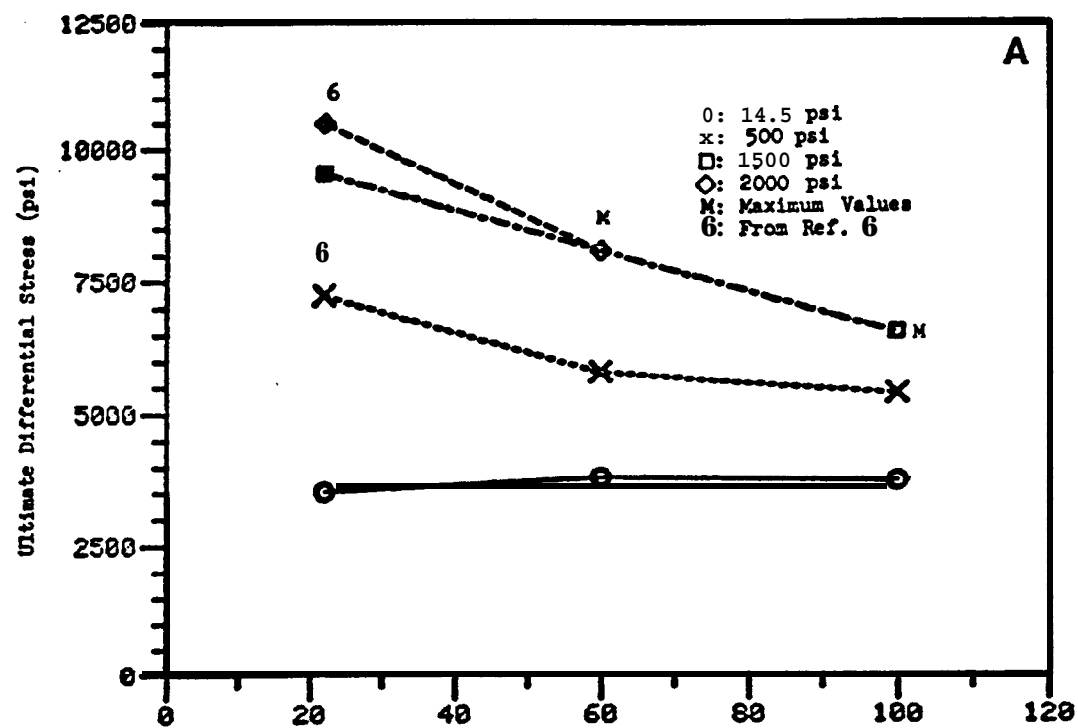
Figure 10: Ultimate differential stress-temperature plots for samples deformed in (A) compression and (B) extension.
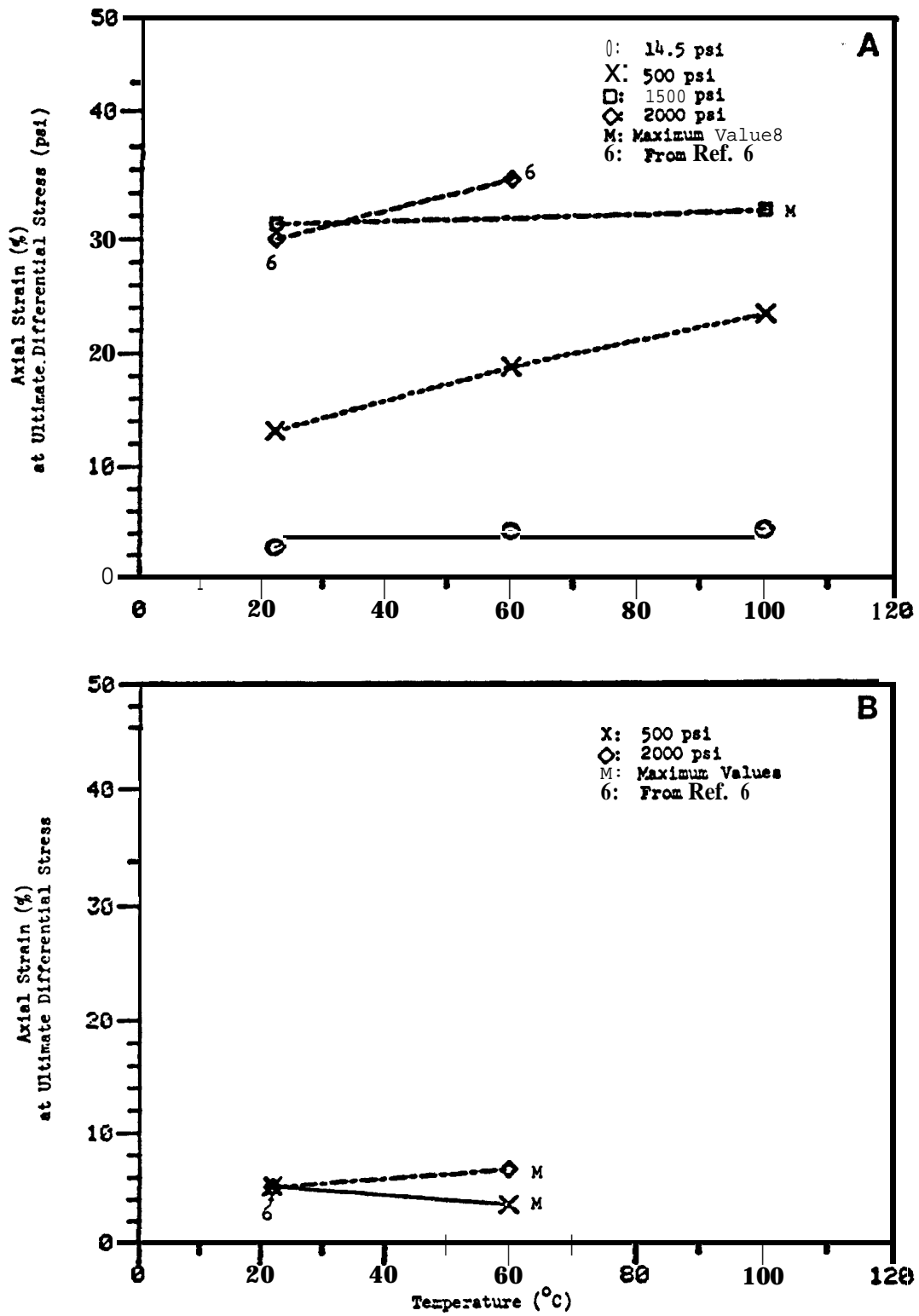
Figure 11:   Axial strain at $\left(\sigma_1 - \sigma_3\right)_u$ temperature plots for samples deformed in (A) compression and (B) extension.

Distribution:

US Department of Energy
Strategic Petroleum Reserve
Project Management Office
900 Commerce Road East
New Orleans, LA   70123
Attn: E. E. Chapple (5)
      C. C. Johnson
      G. A. Stafford
      C. L. Steinkamp

US Department of Energy
Strategic Petroleum Reserve
1000 Independence Avenue SW
Washington, DC   20585
Attn: L. Pettis
      R. Smith

Aerospace Corporation
880 Commerce Road West, Suite 300
New Orleans, LA 70123
Attn: K. Henrie
       R. Merkle

Aerospace Corporation
P. O. Box 92957
Los Angeles, CA   90009
Attn: G. F. Kuncir

Jacobs/D'Appolonia Engineers
6226 Jefferson Hwy., Suite B
New Orleans, LA   70123
Attn: H. Kubicek
       P. Campbell

David K. Parrish
RE/SPEC, Inc.
P. O. Box 725
Rapid City, SD   57701

John W. Handin
Center for Tectonophysics
Texas A&M University
College Station, TX   77843

Neville L. Carter
Department of Geophysics
Texas A&M University
College Station, TX 77843

4000 A. Narath
4500 E. H. Beckner
4512 T. O. Hunter

4512 R. V. Matalucci
4512 D. E. Munson
4540 M. L. Kramm
4543 J. F. Ney
4543 R. R. Beasley
5500 O. E. Jones
5510 D. B. Hayes
5520 T. B. Lane
5521 R. D. Krieg
5522 D. S. Preece
5530 W. Herrmann
5532 B. M. Butcher
5532 D. W. Hannum
5532 R. H. Price (15)
5532 W. R. Wawersik (5)
5532 D. H. Zeuch
5532 J. A. Zirzow
3141 L. J. Erickson (5)
3151 W. L. Garner (3)
3154-3 C. Dalin (25)
       For: DOE/TIC
       (Unlimited Release)
8214 M. A. Pound